CrossMark

ORIGINAL PAPER

Large-scale magmatic layering in the Main Zone of the Bushveld Complex and episodic downward magma infiltration

Ben Hayes[1] · Lewis D. Ashwal[1] · Susan J. Webb[1] · Grant M. Bybee[1]

Abstract The Bellevue drillcore intersects ~3 km of Main and Upper Zone cumulates in the Northern Limb of the Bushveld Complex. Main Zone cumulates are predominately gabbronorites, with localized layers of pyroxenite and anorthosite. Some previous workers, using bulk rock major, trace and isotopic compositions, have suggested that the Main Zone crystallized predominantly from a single pulse of magma. However, density measurements throughout the Bellevue drillcore reveal intervals that show up-section increases in bulk rock density, which are difficult to explain by crystallization from a single batch of magma. Wavelet analysis of the density data suggests that these intervals occur on length-scales of ~40 to ~170 m, thus defining a scale of layering not previously described in the Bushveld Complex. Upward increases in density in the Main Zone correspond to upward increases in modal pyroxene, producing intervals that grade from a basal anorthosite (with 5% pyroxene) to gabbronorite (with 30–40% pyroxene). We examined the textures and mineral compositions of a ~40 m thick interval showing upwardly increasing density to establish how this type of layering formed. Plagioclase generally forms euhedral laths, while orthopyroxene is interstitial in texture and commonly envelops finer-grained and embayed plagioclase grains. Minor interstitial clinopyroxene was the final phase to crystallize from the magma. Plagioclase compositions show negligible change up-section (average An_{62}), with local reverse zoning at the rims of cumulus laths (average increase of 2 mol%). In contrast, interstitial orthopyroxene compositions become more primitive up-section, from Mg# 57 to Mg# 63. Clinopyroxene similarly shows an up-section increase in Mg#. Pyroxene compositions record the primary magmatic signature of the melt at the time of crystallization and are not an artefact of the trapped liquid shift effect. Combined, the textures and decoupled mineral compositions indicate that the upward density increase is produced by the downward infiltration of noritic magma into a previously emplaced plagioclase-rich crystal mush. Fresh noritic magma soaked down into the crystallizing anorthositic mush, partially dissolving plagioclase laths and assimilating Fe-enriched pore melt. The presence of multiple cycles showing upward increases in density in the Bellevue drillcore suggests that downward magma infiltration occurred episodically during crystallization of the Main Zone.

Communicated by T. L. Grove.

✉ Ben Hayes
  ben.hayes@wits.ac.za

[1] School of Geosciences, University of the Witwatersrand, Private Bag 3, Johannesburg 2050, South Africa

Introduction

Large igneous intrusions are commonly characterized by the presence of cyclic/macro-rhythmic layering that is thought to be the product of repeated magma replenishment (e.g., Irvine 1975; Campbell 1977; Bédard et al. 1988). Magma replenishment in a crystallizing chamber has the potential to: (1) reset crystallization sequences, leading to the development of cyclic/macro-rhythmic layering

(O'Hara 1977); (2) trigger the saturation of a new crystal phase due to melt-rock reaction (Lissenberg and Dick 2008; Leuthold et al. 2014; Hayes et al. 2015a); and (3) dissolve existing equilibrium crystal phases, leading to the development of monomineralic cumulates (Bédard and Hébert 1998; O'Driscoll et al. 2010). Each of these processes may account for the formation of phase, modal, and cryptic layering. However, magmatic processes associated with melt migration in crystal mushes may also be involved in developing igneous layering and should be considered when deciphering the formation of layering.

Melt migration in crystal mushes is typically associated with late evolved liquids that are the products of fractional crystallization (Bowen 1928; Boudreau and Philpotts 2002). Buoyant evolved liquids may percolate upward through the crystal mush and accumulate to produce a sandwich horizon (Shirley 1987; Simura and Ozawa 2011). Melt segregation and its upward migration may be driven by compaction of the crystal mush (McKenzie 1984; Shirley 1985). Examples of the upward percolation of evolved melt in layered intrusions have been observed in the Skaergaard intrusion (Humphreys 2009). In the Bushveld Complex, Scoon and Mitchell (2004) described the downward migration of dense, iron-rich melts that formed pipe-like magmatic bodies of iron-rich ultramafic pegmatite (IRUPs). Both Reynolds (1985a) and von Gruenewaldt (1993) proposed a similar mechanism for the development of magnetitite layers in the Bushveld Complex. However, the downward migration of dense, primitive silicate magma has rarely been considered as a significant layer-forming process.

Magmatic layering has been identified throughout the ~8 km vertical thickness of the Bushveld Complex (summarized in Cawthorn 2015). Layering is best exemplified in the Upper Critical Zone, known for its numerous chromitite horizons that host economic quantities of platinum group elements. The Upper Critical Zone has been divided into a series of cyclic units (10's of metres thick) that are typically composed of a basal chromitite, pyroxene-rich cumulates (pyroxenite) that steadily show increasing modal plagioclase upward, culminating in a layer of plagioclase-rich cumulates (anorthosite). Such cyclic units are thought to be the result of gravitational sorting of dense chromite/pyroxene from relatively less dense plagioclase following the injection of a single pulse of magma (Cawthorn and Spies 2003). In terms of bulk rock density, the ideal cyclic unit formed in this way should exhibit upwardly decreasing bulk rock density.

The Bellevue drillcore intersects ~3 km of Upper and Main Zone cumulates of the Bushveld Complex. An extensive petrological, mineralogical, and geophysical database from the drillcore was presented in Ashwal et al. (2005). One of the key findings of this study was the identification of >20 intervals that show upwardly increasing density, a trend that is the opposite of that predicted by the gravitational settling of crystals. The length scales of these upward density increases are on the order of 40–170 m (Webb et al. 2015), which is a scale of layering not previously documented in the Bushveld Complex.

In this study, we present petrological and *in situ* mineral compositional data from a ~40 m thick section of the Bellevue Main Zone that displays upwardly increasing density, defined by an upward increase in modal pyroxene. We suggest that this ~40 m interval was produced when an influx of fresh noritic magma invaded the magma chamber. Dense norite magma drained downwards, soaking into a resident porous anorthositic crystal mush that formed from an earlier injection of plagioclase-rich magma. The occurrence of >20 intervals in the Bellevue drillcore that display upwardly increasing density suggests that downward magma infiltration operated episodically during Main Zone crystallization.

Geological setting

Bushveld complex

The Paleoproterozoic (~2055 Ma; Scoates and Friedman 2008) Bushveld Complex (BC, henceforth) is located in northeast South Africa and covers an area of >100,000 km^2 (Fig. 1). The BC occurs as five major magmatic segments, known as the Eastern, South Eastern (or Bethal), Western, Far Western and Northern Limbs. It was emplaced into the Kaapvaal craton, intruding the Transvaal Supergroup, a predominantly clastic sequence of sedimentary rocks. Recent zircon dating suggests that the BC was emplaced and cooled in <1 M.y. (Zeh et al. 2015). The cumulate stratigraphy of the BC is collectively referred to as the Rustenburg Layered Suite (RLS) and is summarized in Cawthorn (2015). The RLS preserves a complete differentiation sequence of magmatic rocks, from basal peridotites in the Lower and Lower Critical Zones (Cameron 1980; Wilson 2012), to chromitite–norite–anorthosite-dominated cumulates in the Upper Critical Zone (Cawthorn and Spies 2003), to gabbronorites (with local anorthosite and pyroxenite layers) of the Main Zone (Cawthorn et al. 1991; Mitchell et al. 1998; Nex et al. 2002), and finally a sequence of gabbronorite–magnetitite–anorthosite cumulates comprising the Upper Zone (von Gruenewaldt 1973; Tegner et al. 2006).

The Northern Limb of the BC extends along strike for a distance of ~110 km, with a total areal extent of layered mafic cumulate rocks of ~7000 km^2 (van der Merwe 1978; Finn et al. 2015). Mafic cumulates rest upon successively older country rocks of the Pretoria Group
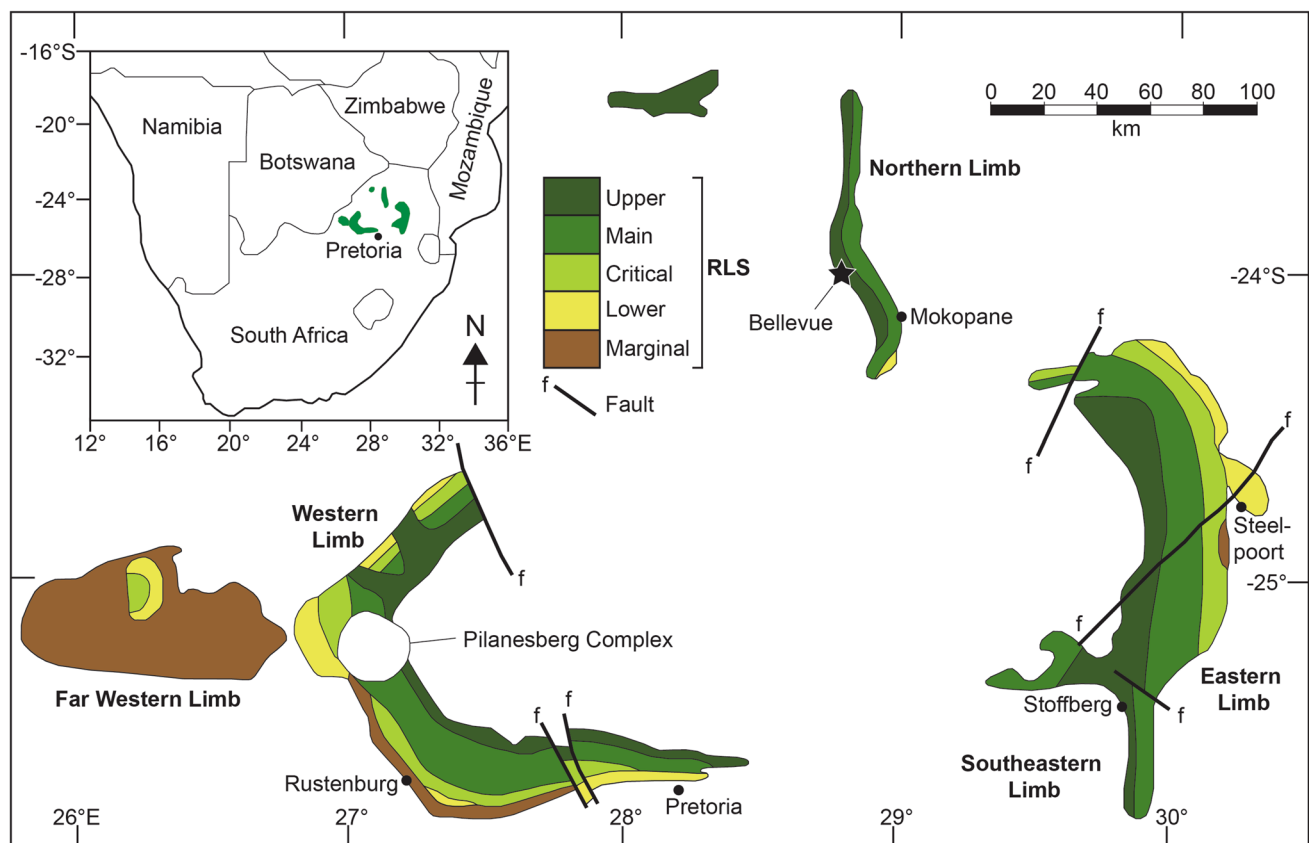
Fig. 1 Simplified geological map of the Bushveld Complex (modified after Cawthorn and Webb 2013). *Inset* shows the location of the Bushveld Complex in South Africa. The location of the Bellevue borehole is shown, in the central part of the Northern Limb, north of Mokopane

towards the north, transitioning from banded iron formations and dolomites of the Chuniespoort Group to Archean granite basement (van der Merwe 1978; Cawthorn 1985). The basal region of the mafic sequence in the Northern Limb comprises a ~400 m package of layered pyroxenites, norites, and anorthosites (with local chromitites) that is known as the Platreef (Kinnaird 2005), which is currently being exploited for platinum group elements.

The Main Zone of the BC is the focus of this study and it is present in the Eastern, Western, and Northern Limbs. In general, the Main Zone is a 2–3 km thick sequence of dominantly gabbronoritic cumulates (Cawthorn 2015). It generally lacks chromite and olivine, both of which are common phases below the Main Zone. Discrete packages of modally layered cumulates have been identified in the Western and Eastern Limbs of the BC (Molyneux 1974; Quadling and Cawthorn 1994; Mitchell et al. 1998; Nex et al. 2002). Near the top of the Main Zone, there is a distinctive layer known as the Pyroxenite Marker that is regarded as being the product of a significant influx of primitive magma at this level of the BC (Cawthorn et al. 1991; Nex et al. 2002; VanTongeren and Mathez 2013). However, no direct equivalent of the Pyroxenite Marker has been observed in the Northern Limb of the BC (Ashwal et al. 2005).

Bellevue drillcore

Our study focuses on the Main Zone from the Northern Limb of the BC, as intersected by the Bellevue drillcore (location marked on Fig. 1). The Bellevue drillcore was collared in roof granites of the BC and it intersects ~3 km of cumulates belonging to Upper and Main Zones. Ashwal et al. (2005) presented a significant database of petrological, mineralogical, magnetic susceptibility and density measurements from the Bellevue drillcore.

A lithological log for the drillcore was provided by Knoper and von Gruenewaldt (1996), later modified by Ashwal et al. (2005). The uppermost 90 m of the drillcore consists of roof granites, which also occur sporadically throughout the drillcore as veins (cm-scale) and sills (up to ~56 m thick), constituting ~10% of the drillcore. The Upper Zone is ~1.2 km thick and it contains ~32 discrete magnetitite layers. The boundary between the Upper and Main Zones is identifiable by a sharp positive peak in magnetic susceptibility that is caused by the presence of significant

modal magnetite at this stratigraphic level (Ashwal et al. 2005). The Bellevue Main Zone is ~1.4 km thick and it is dominated by gabbronoritic cumulates with local pyroxenite and anorthosite layers. At the base of the Main Zone in the Bellevue drillcore is an unusual troctolite horizon that was mapped by van der Merwe (1978) for ~35 km along strike in the Northern Limb. The Moordkopje drillcore (presented in Roelofse and Ashwal 2012) intersects Main Zone cumulates below the base of the Bellevue drillcore, extending the thickness of the Main Zone to ~3 km, giving a comparable thickness to that observed in the Eastern and Western Limbs of the BC.

Analytical Methods

Mineral compositions were acquired using a Cameca SX five field-emission electron microprobe at the University of the Witwatersrand. All *in situ* mineral compositions were measured using an acceleration potential of 15 kV and with a current of 20 nA. A focused beam was used for pyroxene analyses, while a defocused beam of 5 μm diameter was used for plagioclase. All totals that were outside the range 98.5–101.5 wt% were discarded. Core and rim analyses were generally measured for all phases to characterize compositional zonation. More detailed profiles were also conducted across various grains to check for any complex zoning. The full data set is provided in Appendix 1. Element maps for some samples were run for ~5 h using the same conditions as spot analysis.

Bulk rock density cyclicity and length-scales

Bulk rock density measurements were recorded at depth intervals of 1 to 1.5 m throughout the Bellevue drillcore, totalling 2252 measurements. The complete data set (including uncertainties) can be found in Ashwal et al. (2005). Bulk density ranges from ~2.65 g/cm^3 to 4.50 g/cm^3 throughout the Bellevue drillcore (Fig. 2). Rocks with the lowest densities (~2.65 g/cm^3) correspond to plagioclase-rich cumulates (anorthosites with >90% plagioclase) as well as minor granite intrusions. Bulk rock densities of >3 g/cm^3 typically correspond to pyroxene-rich cumulates (pyroxenites with >60% pyroxene). Bulk rock densities >3.5 g/cm^3 contain appreciable modal magnetite and predominantly occur in the Upper Zone (boundary marked on Fig. 2).

Bulk rock density measurements throughout the entire Bellevue drillcore reveal a cyclicity that is characterized by both upward decreases and upward increases in density (Fig. 2). There are also intervals that show negligible change in density up-section (Fig. 2). There are
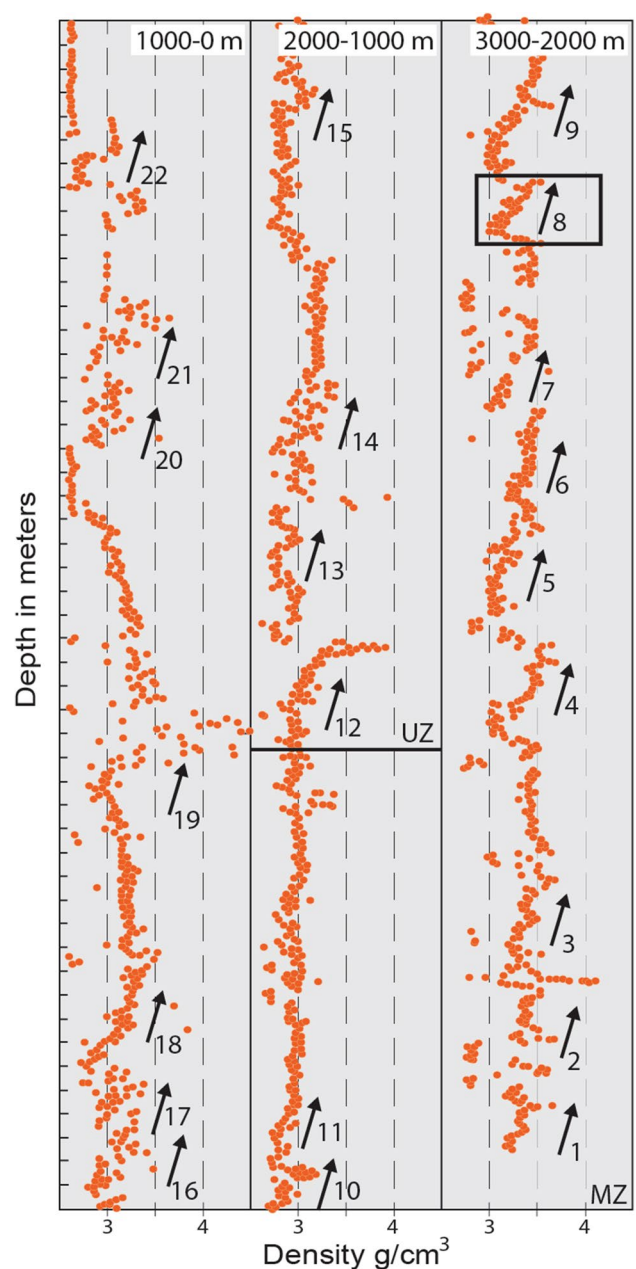

Fig. 2 Bulk rock density measurements through the entire Bellevue drillcore (modified after Ashwal et al. 2005). Note that there are > 20 intervals (*labelled*) showing upwardly increasing bulk rock density. Interval 8 (2175–2140 m) is the focus of this paper (shown in *box*). Ticks on the *y*-axis correspond to 20 m intervals. *UZ* upper zone, *MZ* main zone

approximately 22 cycles, where bulk density increases upward (labelled on Fig. 2). Cycles displaying upward increases in bulk rock density are of interest, because such trends are the opposite of that predicted by traditional magma fractionation produced by gravity sorting.

The periodicity of cycles displaying upwardly increasing density has been analyzed using wavelet analysis

(Webb et al. 2015), which enables the variation of the frequency content with depth to be determined, allowing the calculation of the average periodicity with depth. The results reveal a periodicity signal varying between ~40 and ~170 m for cycles showing upwardly increasing density (Webb et al. 2015). The length scales and periodicity of these cycles are on a scale not previously documented in the BC. In addition, upwardly increasing density is not visibly apparent to the eye upon inspection of the drill-core or in surface exposures, highlighting the importance of systematically measuring bulk density in drillcore material.

In this study, we focus on a ~40 m interval (interval 8 on Fig. 2), which begins at ~2175 m depth. We selected this interval, because it represents a well-sampled sequence of cumulates that display upwardly increasing density. We use petrography and mineral chemistry to develop an interpretive model to explain the origin of such layering.

Petrography

The base of interval 8 (~2175 m; Fig. 2) consists of anorthosites with 90% plagioclase and 10% pyroxene, which is dominantly orthopyroxene. Plagioclase forms coarse (~4–6 mm) euhedral laths (Fig. 3a). These crystals generally display triple-junction grain boundaries with neighbouring plagioclase laths, with minor amounts of interstitial plagioclase at these grain boundaries (Fig. 3a). Both orthopyroxene and clinopyroxene are interstitial to plagioclase and texturally appear to have crystallized from pore melt between the plagioclase laths (Fig. 3a–f). Orthopyroxene commonly

Fig. 3 Photomicrographs of the textures observed in interval 8. **a** A euhedral plagioclase lath (Pl) in the basal region of interval 8. In addition, note some minor interstitial plagioclase (*white arrow*) at the junction between cumulus plagioclase laths. **b** Interstitial orthopyroxene (Opx) enclosing rounded plagioclase grains. Orthopyroxene is surrounded by euhedral plagioclase laths. **c** Interstitial orthopyroxene enclosing rounded and corroded plagioclase grains. There are small (~0.1 mm) inclusions of clinopyroxene within the orthopyroxene grain that may be caused by exsolution. Polysynthetic twins in the labelled plagioclase lath are bent, suggesting minor amounts of compaction. **d** Partly enclosed plagioclase lath with embayed margins (*black arrows*) surrounded by interstitial orthopyroxene. **e** Interstitial orthopyroxene enclosing a rounded (margins shown with *white arrows*) plagioclase grain. In addition, note the presence of interstitial clinopyroxene (Cpx). **f** Euhedral orthopyroxene grain that is partly embayed. The euhedral orthopyroxene grain is surrounded by a corona of clinopyroxene (*white arrows*). Note the inverted pigeonite (Ipx) grain
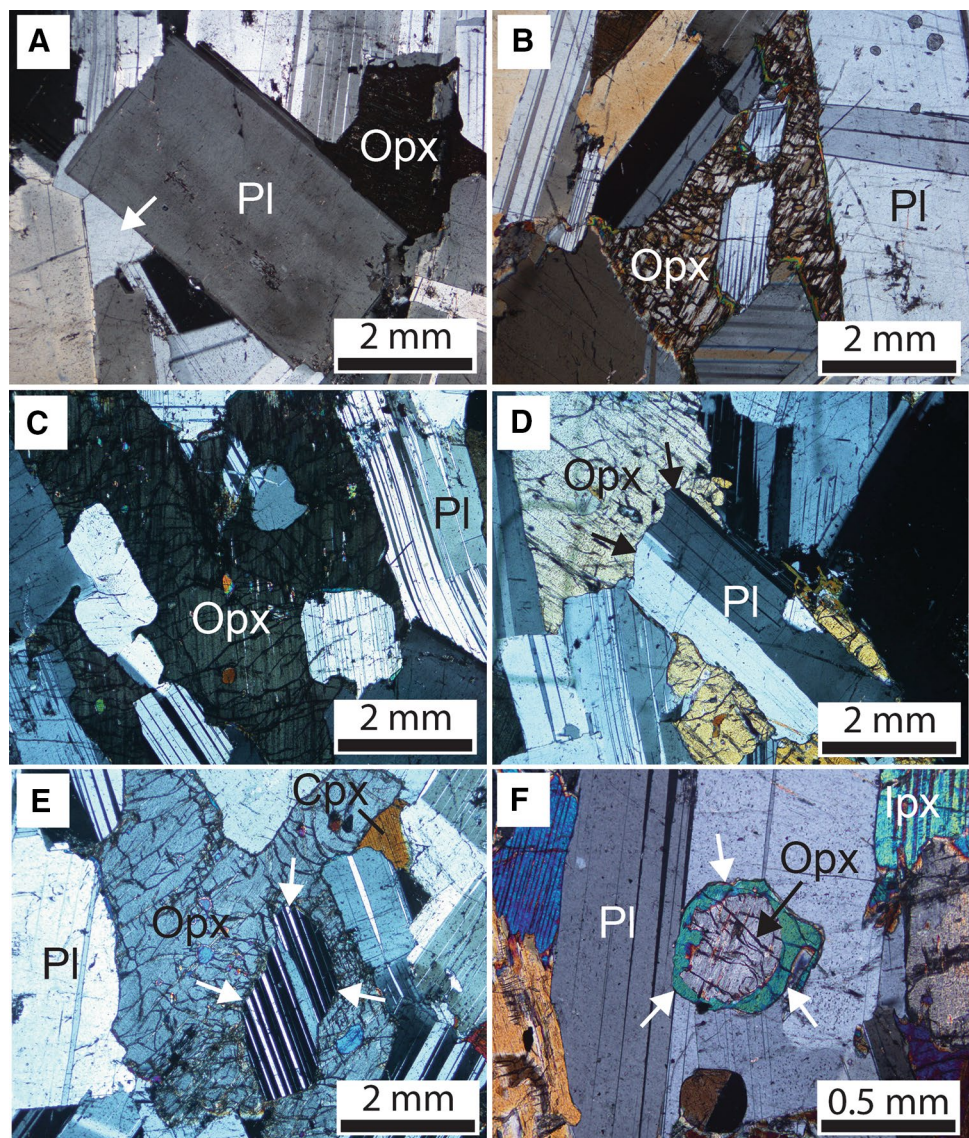
encloses fine-grained (1–2 mm) plagioclase grains, locally developing a poikilitic texture (Fig. 3b–e) that suggests some early orthopyroxene crystallization when plagioclase was still crystallizing from the magma. Enclosed plagioclase crystals within orthopyroxene oikocrysts are typically rounded and embayed (Fig. 3b–e) compared to larger, euhedral plagioclase laths that are not enclosed by orthopyroxene. Clinopyroxene typically produces triangular-shaped grains (Fig. 3e), suggesting that it was the final phase to crystallize from the magma.

Progressively up-section in interval 8, plagioclase remains the dominant phase (up to ~75%) and continues to occur as coarse euhedral laths. Orthopyroxene gradually increases in abundance upward (eventually reaching modes of ~15–20%), and remains interstitial in texture to the euhedral plagioclase laths (Fig. 3d-f). Poikilitic textures are locally prominent, with orthopyroxene enclosing rounded and embayed plagioclase grains. Clinopyroxene (~5–10%) also remains interstitial in texture, typically forming anhedral grains (Fig. 3e), consistent with its crystallization from late pore melt. Locally, there are occurrences of fine-grained (~1 mm), euhedral orthopyroxene grains. Such occurrences of euhedral orthopyroxene grains are partly embayed and in some instances are mantled by clinopyroxene (Fig. 3f). Inverted pigeonite becomes more common up-section in interval 8 as the modal proportion of orthopyroxene increases (Fig. 3f).

Mineral compositions

In general, An content [atomic $Ca/(Ca+Na+K)\times100$] of plagioclase displays negligible up-section change in interval 8 (Fig. 4a). Representative analyses are shown in Table 1. The cores of euhedral plagioclase grains throughout interval 8 range between An_{67} and An_{60}, with an average value of An_{62}. The core compositions of finer-grained and rounded plagioclase grains that are enclosed by orthopyroxene are slightly more primitive (An_{63}) than euhedral plagioclase laths. FeO in plagioclase shows a gradual up-section enrichment in interval 8 with an increase from 0.4 to 0.6 wt% (Appendix 1). Euhedral plagioclase laths are typically normally zoned (becoming more evolved from core to rim) with typical decreases of 1–2 mol% An at the rim. Reverse zoning is also observed, in both euhedral plagioclase laths and plagioclase grains that are enclosed by orthopyroxene. The average increase is 2 mol% An at the rims of reversely zoned grains with local increases of up 10 mol% An observed from core to rim (Fig. 5). Such extreme reverse zoning has been reported in the Bushveld Complex and other layered intrusions (Morse and Nolan 1984), and may be interpreted as plagioclase crystallization in the presence of minor H_2O-bearing melt pockets (Boudreau 1988).

The Mg# [atomic $Mg/(Mg+Fe+Mn)\times100$] of orthopyroxene displays a gradual up-section increase in interval 8 (Fig. 4b). Representative analyses for orthopyroxene are shown in Table 2. Orthopyroxene Mg# increases from 57 in the basal anorthosites to 63 in the upper gabbronorites. Orthopyroxene is typically unzoned, with minimal Mg# changes from the cores to rims of individual grains. For instance, where zonation is present, it is generally characterized by normal zoning with the largest core to rim change in Mg# of ~2 mol%. Clinopyroxene Mg# also displays an up-section increase (Fig. 4c), with Mg# increasing from 65 to 72. Clinopyroxene typically displays core to rim zonation, with normal zoning most commonly observed

Fig. 4 Mineral compositional profiles plotted as a function of stratigraphic height through interval 8. **a** Molar An content of plagioclase (total number of analyses = 275). **b** Molar Mg# of orthopyroxene (total number of analyses = 51). **c** Molar Mg# of clinopyroxene (total number of analyses = 81). Red dots are the mean core value and the black line denotes the range of compositions analyzed at each height (full database included in Appendix 1). Also shown is the modal proportion of phases throughout Interval 8
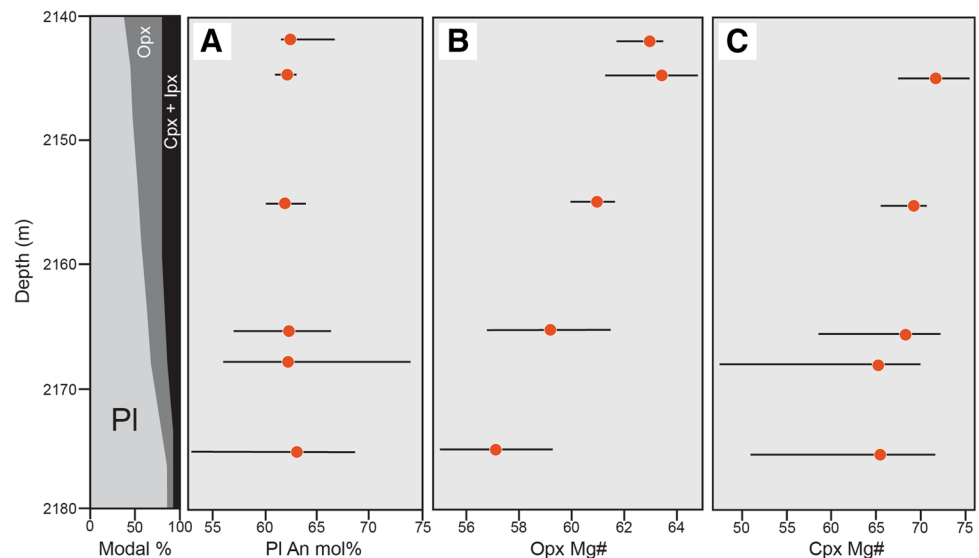
Table 1 Representative electron microprobe analyses of plagioclase from Interval 8 of the Main Zone

Depth (m)	2175.20	2175.20	2167.90	2167.90	2144.85	2144.85	2142.07	2142.07
Rock type	Anorthosite	Anorthosite	Leuconorite	Leuconorite	Gabbronorite	Gabbronorite	Gabbronorite	Gabbronorite
Morphology	Resorbed chad	Resorbed chad	Lath	Lath	Lath	Lath	Chad	Chad
Crystal region	Core	Rim	Core	Rim	Core	Rim	Core	Rim
SiO_2	51.56	48.08	52.55	51.37	52.76	52.04	51.62	51.4
TiO_2	0.02	0.02	0.04	0.02	0.05	0.02	0.03	0.02
Al_2O_3	30.25	32.64	29.84	30.54	29.69	30.4	29.86	30.04
MgO	0	0	0	0	0	0	0	0
CaO	12.8	15.33	12.16	12.54	12.04	12.32	12.54	12.66
MnO	0.04	0	0	0.02	0.01	0	0	0
FeO	0.3	0.37	0.4	0.38	0.42	0.38	0.41	0.5
Na_2O	4.08	4.03	4.32	3.95	4.1	3.98	3.95	3.84
K_2O	0.19	0.18	0.2	0.2	0.25	0.22	0.21	0.24
BaO	0.1	0	0.02	0.01	0.01	0.02	0	0.03
SrO	0	0	0	0	0	0	0	0
Total	99.25	100.65	99.53	99.03	99.33	99.38	98.62	98.71
An mol%	62.7	67.1	60.1	62.9	60.9	62.3	62.9	63.6

Core centre of crystal, *Rim* edge of crystal, *Chad* chadacryst enclosed by orthopyroxene
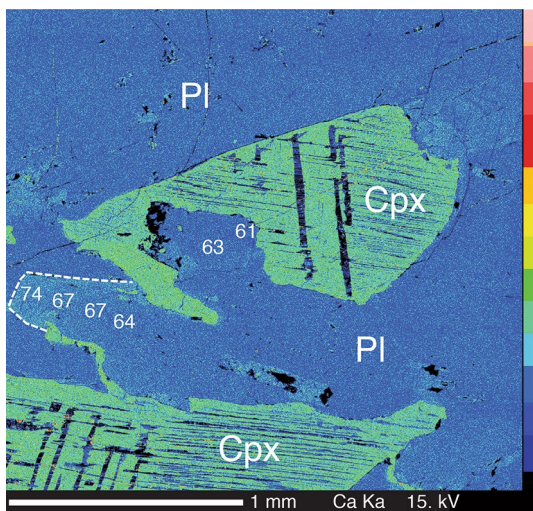

Fig. 5 Calcium element X-ray map of a reversely zoned plagioclase lath from 2167.90 m depth (dashed *white line* indicates the margin of the lath). The molar An content of the plagioclase lath increases from An_{64} in the core to An_{74} at its rim. Such extreme local An zonation may be caused by the presence of H_2O-bearing melt pockets during crystallization. In addition, note the interstitial clinopyroxene grain with orthopyroxene exsolution lamellae

(typically with shifts of 2 mol% in Mg#). Reverse zoning in interstitial clinopyroxene is also observed, with shifts in Mg# of up 4 mol% observed from core to rim. Representative clinopyroxene analyses are shown in Table 3. The presence of local reverse zoning in plagioclase and clinopyroxene suggests that the interval did not crystallize as a closed system from a single batch of magma.

Discussion

Previous crystallization models for the Main Zone

The Main Zone (and Upper Zone) of the BC is typically regarded as being the result of closed-system fractional crystallization (Wager and Brown 1968; von Gruenewaldt 1973; Molyneux 1974; Maier and Barnes 1998). Tegner et al. (2006) proposed that the Main and Upper Zones were the product of the crystallization of a huge sheet of initially homogeneous magma that was >2 km in thickness. During crystallization of this magma sheet, double-diffusive convection operated with magnetitite–gabbronorite crystallization driving the production of less dense melts, which led to mixing between the basal layer and the top of the magma chamber. Reversals in mineral compositions were attributed to such a mixing process. The model of Tegner et al. (2006) is reminiscent of that proposed by Reynolds (1985a) and von Gruenewaldt (1973) for the formation of magnetitite layers. Mixing events caused by double-diffusive convection would have occurred periodically during the crystallization of the Main Zone (Tegner et al. 2006). Tegner et al. (2006) also argue that their model is consistent with bulk Sr initial isotopic ratios that show little up-section change ($Sr_i = 0.7071–0.7074$) in the Main Zone. However, it is possible that multiple magmas with the same bulk isotopic signature were emplaced into the BC.

In opposition to closed-system crystallization models for the origin of the Main Zone, Mitchell et al. (1998) provided textural and mineral compositional evidence for periodic replenishment of the Main Zone in the Western

Table 2 Representative electron microprobe analyses of orthopyroxene from Interval 8 of the Main Zone

Depth (m)	2175.20	2175.2	2165.45	2165.45	2165.45	2144.85	2144.85	2142.07	2142.07
Rock type	Anorthosite	Anorthosite	Leuconorite	Leuconorite	Leuconorite	Gabbronorite	Gabbronorite	Gabbronorite	Gabbronorite
Morphology	Interstitial	Interstitial	Interstitial	Interstitial	Interstitial	Interstitial	Interstitial	Interstitial	Interstitial
Crystal region	Core	Core	Core	Core	Rim	Core	Core	Core	Rim
SiO_2	50.90	51.19	51.3	51.52	51.12	52.25	52.03	50.1	50.54
Al_2O_3	0.59	0.57	0.76	0.74	0.7	0.9	0.77	0.88	0.69
FeO	27.39	28.53	26.27	26.25	27.19	24.13	23.74	23.11	24.1
TiO_2	0.17	0.09	0.25	0.27	0.21	0.22	0.2	0.22	0.23
Cr_2O_3	0.02	0.01	0.01	0.02	0	0.02	0.02	0.01	0.04
MgO	20.77	19.62	20.97	21.22	20.09	21.42	23.32	22.54	22.77
MnO	0.58	0.61	0.57	0.58	0.61	0.59	0.47	0.48	0.49
CaO	0.74	0.57	0.83	0.79	0.8	0.8	0.72	1.56	0.8
NiO	0	0	0	0	0	0	0	0	0
Na_2O	0.02	0.03	0.02	0.02	0.01	0.04	0	0.02	0.1
K_2O	0	0	0	0.01	0	0.04	0	0	0
Total	101.18	101.22	100.98	101.42	100.73	100.41	101.27	98.9	99.67
Mg#	57.5	55.1	58.7	59.0	56.8	61.3	63.6	63.5	62.7

Core centre of crystal, *Rim* edge of crystal

Table 3 Representative electron microprobe analyses of clinopyroxene from Interval 8 of the Main Zone

Depth (m)	2175.20	2175.20	2175.20	2167.90	2165.45	2165.45	2144.85	2144.85
Rock type	Anorthosite	Anorthosite	Anorthosite	Leuconorite	Leuconorite	Leuconorite	Gabbronorite	Gabbronorite
Morphology	Interstitial	Interstitial	Interstitial	Interstitial	Interstitial	Inclusion in opx	Interstitial	Interstitial
Crystal region	Core	Core	Core	Core	Rim	Core	Core	Core
SiO_2	51.01	51.25	50.95	52.31	51.06	51.24	51.21	51.08
Al_2O_3	1.52	1.19	1.9	0.73	1.84	1.47	1.67	1.89
FeO	10.77	10.31	10.47	11.03	10.95	10.5	10.63	9.7
TiO_2	0.38	0.29	0.33	0.12	0.5	0.45	0.38	0.44
Cr_2O_3	0	0	0.02	0	0	0.02	0.04	0.02
MgO	13.39	13.38	13.52	13.48	13.34	13.61	14.24	13.81
MnO	0.26	0.27	0.29	0.35	0.27	0.22	0.27	0.21
CaO	21.0	21.76	20.93	21.22	20.56	21.18	19.98	21.32
NiO	0	0	0	0	0	0	0	0
Na_2O	0.21	0.18	0.25	0.18	0.27	0.23	0.23	0.28
K_2O	0	0.01	0	0	0.01	0	0	0.1
Total	98.54	98.64	98.66	99.42	98.8	98.92	98.65	98.76
Mg#	68.9	69.8	69.7	68.5	68.5	69.8	70.5	71.7

Core centre of crystal, *Rim* edge of crystal, *Opx* orthopyroxene

Limb. They described corroded plagioclase inclusions within orthopyroxene, as well as up-section increases in orthopyroxene Mg# that they ascribed to the gradual mixing of small influxes of fresh magma with a resident, more evolved magma containing plagioclase. Sharpe (1981) proposed that the Main Zone intruded as a crystal mush between the Critical Zone and the upper region of the Main Zone (above the Pyroxenite Marker), based on bulk Sr isotope data. In this model, the upper Main Zone represents the differentiated products of the Lower and Critical Zones. A similar model involving crystal-rich or mushy magmas was proposed by Roelofse and Ashwal (2012) for the lower region of the Main Zone in the Northern Limb as intersected by the Moordkopje drillcore. They envisioned influxes of crustally contaminated plagioclase and orthopyroxene slurries from a deeper staging chamber.

There is further evidence for magma replenishment in the Main Zone. For instance, the Pyroxenite Marker in the

Western Limb provides compelling evidence for a major influx of orthopyroxene-saturated magma into the Main Zone (Cawthorn et al. 1991). Nex et al. (2002) provided a detailed description of the style of magma replenishment at the Pyroxenite Marker. They noted that plagioclase shows an up-section increase towards more primitive An compositions and orthopyroxene Mg# shows no up-section change. This decoupling in mineral compositions was thought to be caused by variations in the degree of mixing between influxes of new melt with a more evolved resident pore melt (Nex et al. 2002). Based on these decoupled mineral compositional trends, they suggested that magma replenishment was a gradual process, with incremental magma addition and mixing with resident magma in the chamber, culminating in a mass influx of orthopyroxene-saturated magma to produce the Pyroxenite Marker. VanTongeren and Mathez (2013) proposed a similar model for the formation of the Pyroxenite Marker. They suggested that a series of small, gradual magma influxes were emplaced into a chemically homogeneous magma body. The rate of magma emplacement was slow enough to allow the magma body to homogenize and partially crystallize between magma influxes.

In summary, there is abundant evidence to suggest that magma replenishment was an important process during the crystallization of the Main Zone. In the following discussion, we will synthesize the textural and mineral compositional constraints from interval 8 in the Bellevue drillcore to test whether the various models described above could account for the cycles showing upwardly increasing density. We will then provide an alternate model for the origin of this cyclicity.

Textural constraints on the crystallization of interval 8

The textures observed in interval 8 provide important insights into the nature of crystallization and the formation of the upward increase in density. Plagioclase is the dominant phase and it appears to be cumulus in nature, forming euhedral laths throughout interval 8 (Fig. 3). In contrast, plagioclase grains that are enclosed by orthopyroxene are typically rounded. Both Eales et al. (1991) and Mitchell et al. (1998) suggested that rounded or embayed plagioclase grains in BC cumulates were produced by the partial dissolution of pre-existing plagioclase grains that were exposed to a fresh influx of hotter magma. We also suggest that rounded and embayed plagioclase grains enclosed by orthopyroxene were partially dissolved and are, therefore, not in equilibrium with their host orthopyroxene grain. This suggests that the host orthopyroxene grains crystallized from a discrete magma to that from which the enclosed plagioclase crystallized.

Another important textural constraint on the crystallization of interval 8 is that orthopyroxene is dominantly interstitial in texture. Orthopyroxene is a major phase throughout the BC, and it commonly forms euhedral primocrysts. However, the interstitial nature of orthopyroxene in interval 8 suggests that it crystallized from pore melts associated with the euhedral plagioclase laths. Orthopyroxene that encloses fine-grained and corroded plagioclase grains would have crystallized from the pore melt during crystallization of interval 8, arresting the growth of the enclosed and resorbed plagioclase grains. Entrapment of plagioclase by orthopyroxene appears to have taken place relatively early in the development of the mush, because some of the most primitive plagioclase compositions are preserved in chadacrysts enclosed by orthopyroxene oikocrysts. Clinopyroxene is anhedral and typically forms triangular-shaped grains at triple-grain junctions, indicating that it was the final phase to crystallize from the pore melt. Locally, fine-grained, euhedral orthopyroxene grains may represent primocrysts (Fig. 3f) that did not crystallize *in situ* from the pore melt. These primocrystic orthopyroxene grains have coronas of clinopyroxene, suggesting that they interacted with a melt that was crystallizing clinopyroxene at a later stage.

The corroded texture of the plagioclase grains enclosed by orthopyroxene, combined with the dominantly interstitial texture of orthopyroxene, suggests that interval 8 crystallized from two main components: (1) an initial plagioclase-rich crystal mush and (2) a magma that crystallized orthopyroxene (a minor component of which is primocrystic and may have been entrained in this magma), as well as late plagioclase and clinopyroxene.

Mineral compositions: trapped liquid shift effect or decoupling?

The upward increase in molar Mg# of orthopyroxene and clinopyroxene (Fig. 4b, c) in interval 8 suggests that both these phases crystallized from increasingly more primitive melt up-section. However, it could argued that this upward increase in Mg# is a product of the trapped liquid shift effect (TLSE; Barnes 1986; Cawthorn et al. 1992). During the TLSE, cumulus ferromagnesian phases exchange Fe and Mg with trapped pore melt, increasing the Fe/Mg ratio of the cumulus ferromagnesian phase. The TLSE is proportional to the modal amount of the ferromagnesian phase in the rock, such that when the ferromagnesian phase is present in low modal abundances, the increase in Fe/Mg of that phase is greater. The most evolved compositions of orthopyroxene and clinopyroxene occur at the base of interval 8, where the modal abundance of these phases is lowest, consistent with that predicted by the TLSE. However, both orthopyroxene and clinopyroxene are interstitial phases in interval 8 and thus crystallized from pore melt; therefore, they likely represent the composition of that pore melt

at the time of crystallization. In addition, if the TLSE is responsible for the mineral compositional trends observed in both orthopyroxene and clinopyroxene, then this would require that the original Mg# profile mirrored the compositional trend shown by An in plagioclase, with no up-section mineral composition evolution. This is a problem in itself, as it is difficult to produce a 40 m thick package of cumulates that shows no up-section compositional evolution for multiple phases.

We calculated the proportion of trapped melt required at the base of interval 8 to cause the shift from the most primitive orthopyroxene core composition (Mg# 63) to the average orthopyroxene core composition (Mg# 57) in the basal region of interval 8 (schematically shown in Fig. 6). Such a calculation assumes no melt migration during crystallization. It is possible that compaction enabled minor amounts of pore melt to escape (Meurer and Boudreau 1998). Bent twins in plagioclase (Fig. 3a) provide evidence for compaction at the base of interval 8; however, it is difficult to quantify the exact proportions of melt lost. We calculated an appropriate Fe/Mg exchange coefficient (Kd) between orthopyroxene and melt using the method of Bédard (2007). We used a Kd value of 0.25, consistent with a melt containing ~6 wt% MgO, which is appropriate for this level of the Main Zone (VanTongeren and Mathez 2013). Using the Fe/Mg ratio of orthopyroxene, combined with the Kd value, we calculated the proportion of trapped melt required to cause a shift from Mg# 63 to Mg# 57. A trapped melt content of ~20% is required to be present at the base of interval 8 (Fig. 6). However, <10% interstitial material, which would have crystallized from trapped melt, is present at the base of interval 8. In addition, no significant normal zonation is observed in plagioclase at this level of interval 8 that would indicate it crystallized in the presence of an

evolved trapped melt whereas this has been observed in other parts of the BC (Maier & Eales 1998; Ashwal et al. 2005).

Plagioclase faithfully preserves the melt composition at the time of crystallization, because the diffusive exchange of Ca-Al and Na-Si between crystal and melt is extremely slow at magmatic temperatures (Morse 1984). The lack of up-section evolution in plagioclase An content indicates that there was no change in the composition of the melt from which plagioclase crystallized. The minimal core to rim zoning of Mg# in pyroxene suggests that there was partial resetting and re-equilibration of pyroxene with trapped melt, but only on a local grain scale, where grains were in contact with pockets of late-stage pore melt. The overall Mg# profile in pyroxene was not produced by interaction with trapped melt, and is, therefore, decoupled from the compositionally homogeneous plagioclase grains.

In summary, we posit that the up-section Mg# trends observed in both orthopyroxene and clinopyroxene are primary magmatic compositions and are representative of the melt composition at the time of crystallization. Melt compositions thus become more primitive up-section in interval 8. Plagioclase and pyroxene compositions are, therefore, decoupled, a factor that must be considered when developing a model for the crystallization of interval 8.

A model for the formation of upward density increases in the Main Zone

Initial injection of a plagioclase-rich crystal mush

In the study of Roelofse and Ashwal (2012), it was proposed that the lowermost region of the Main Zone in the Northern Limb of the BC was emplaced as a series of

Fig. 6 Schematic diagram illustrating how the trapped liquid shift effect (TLSE) would have produced the mineral compositions observed in Interval 8. An initial profile would show negligible up-section change in plagioclase (Pl) An content and pyroxene (Px) Mg#. The proportion of trapped melt required to cause a shift from the most primitive Mg# to the most evolved Mg# in interval 8 is ~19% (see text for details of the calculation). Such a proportion of trapped melt would produce the final profile showing an up-section increase in pyroxene Mg# and its compositional decoupling from plagioclase
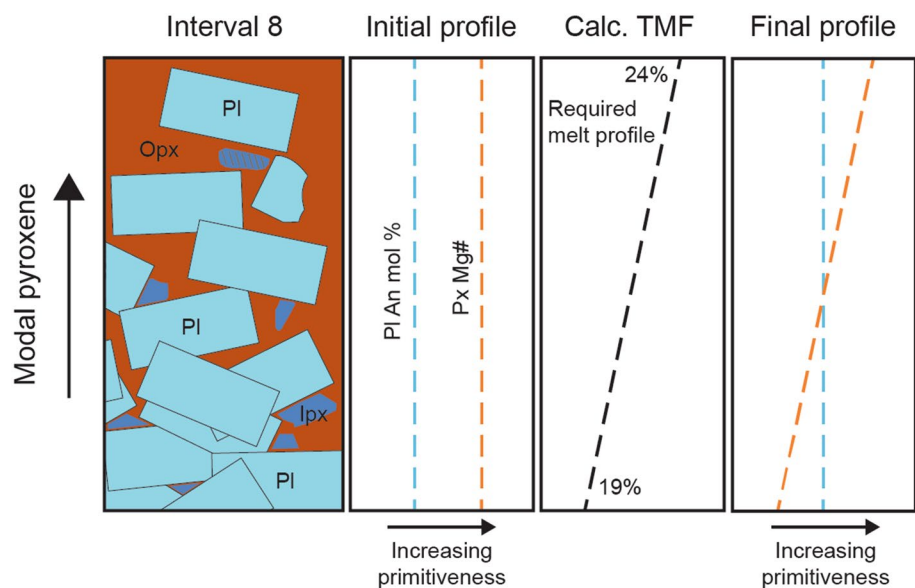
crystal mushes. This assertion was partly based on the lack of An compositional evolution in plagioclase and Mg# of pyroxene over >1 km of cumulate stratigraphy. We also observe a lack of An compositional evolution in interval 8, and combined with the non-cotectic proportions of plagioclase, we propose that a significant proportion of plagioclase in interval 8 was emplaced as a crystal mush. A similar style of emplacement was proposed for thick, discrete layers of anorthosite in the Stillwater Complex. For example, on the basis of (a) large plagioclase grain sizes, (b) complex zoning, (c) lack of internal stratification/layering, and (d) the lack of An evolution up-section, it was suggested that anorthosite layers in the Stillwater Complex initially formed as thick plagioclase-liquid mushes (Czamanske and Bohlen 1990; McCallum 1996). Foose (1985) noted that anorthosite layers in the Stillwater Complex were transgressive and contained blocks of host troctolitic rocks, supporting its emplacement as a plagioclase-rich crystal mush. More recent evidence from the BC indicates that transgressive anorthosite packages formed by the mobilization of plagioclase slurries (Maier et al. 2016). The emplacement of plagioclase-phyric magmas has also been proposed for the Cuillin magma chamber on the Isle of Skye (Brandriss et al. 2014). The remobilization of plagioclase-rich crystal mushes and their subsequent injection into higher-level magma chambers may, therefore, be a fundamental process during the construction of layered intrusions (Ashwal 1993).

In interval 8, an initial pulse of a plagioclase-rich crystal mush, with an average composition of An_{62}, would have been emplaced into the resident magma chamber. It is not possible for us to determine the exact plagioclase-melt ratio of this mush, but experimental studies would suggest of upper limit of 50% crystals (Marsh 1981). The injection of a plagioclase crystal mush into the Main Zone of the BC also implies that there was pre-modification of Main Zone magmas deeper in the crust, beneath the level of the BC magma chamber. Studies by Mondal and Mathez (2007) and Eales and Costin (2012) have posited similar deeper plumbing mechanics of magma for the origin of chromitite layers in the Upper Critical Zone. In contrast, Maier et al. (2013) proposed that within-chamber mobilization and sorting of crystal mushes were responsible for the formation of cumulate layering. In either case, there exists ample evidence that the emplacement of crystal mushes and slurries was an important process during construction of the BC.

Downward infiltration of noritic magma

The upwardly increasing modal pyroxene content (dominantly orthopyroxene) of interval 8 can be best explained by the downward infiltration of a fresh pulse of noritic magma. An influx of noritic magma would have been relatively denser than the earlier emplaced plagioclase-rich crystal mush and would, therefore, have drained into the resident mush (Fig. 7). We conducted a simple model to determine the density relations between the anorthositic mush and the noritic magma. Liquidus phase densities were estimated from a MELTS run of the B3 melt composition, thought to be a candidate for the parental melt of the Main Zone (Barnes et al. 2010). The density of the melt phase in the noritic magma was assumed to be basaltic in composition (2.7 g/cm^3), while a slightly denser melt composition (2.9 g/cm^3) was estimated for the anorthositic mush due to its iron-rich pore melt composition (Ashwal 1993). We found that a noritic magma carrying an entrained cargo of orthopyroxene crystals as low as 10-vol% would have been more dense than a resident anorthositic mush containing 50-vol% plagioclase crystals (upper limit of crystallinity for a flowing magma; Marsh (1981)).

As the infiltrating noritic magma propagated downwards, it would have mixed with iron-rich pore melt associated with the anorthositic mush. The mixed magma at the leading edge of the infiltrating magma front would have crystallized relatively evolved orthopyroxene (Mg# 57) and clinopyroxene (Mg# 65) in the pore spaces between euhedral plagioclase grains. The up-section increase in Mg# of orthopyroxene and clinopyroxene is, therefore, a function of a lesser component of resident iron-rich pore melt associated with the anorthositic mush. Euhedral orthopyroxene grains that are present in a low abundance in interval 8 may represent primocrystic phases that were delivered into the chamber with the invading norite magma (e.g., Hatton 1988). Downward percolating magma may have transported primocrystic orthopyroxene grains deeper into the anorthosite mush. The mixing relations between the noritic magma and the resident iron-rich pore melt would have facilitated the downward propagation of magma by increasing the density of the invading noritic magma. Combined with the density relations, downward magma infiltration would have been promoted by chemical disequilibrium between the noritic magma and the anorthositic mush. The presence of corroded plagioclase grains enclosed by orthopyroxene oikocrysts can be explained by dissolution of early formed plagioclase grains. Dissolution would have been caused by a chemically discrete noritic magma ingesting the resident anorthositic mush, further promoting magma infiltration. Localized reverse zoning in plagioclase can also be explained by plagioclase laths interacting with a slightly more primitive magma having a slightly higher Ca/Na ratio. Reversely zoned clinopyroxene grains may also record this interaction. In both cases, the interaction of relatively primitive melt with the resident pore melt would have prevented the formation of normal zoning in plagioclase. More extreme examples of reverse zonation that we
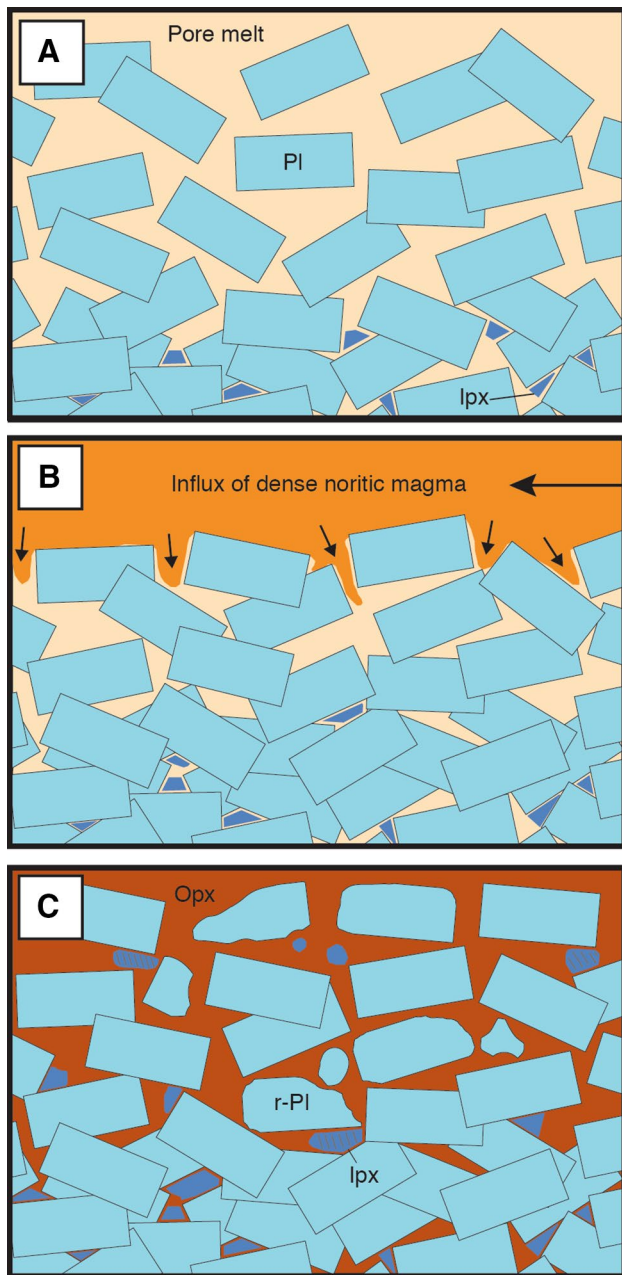
Fig. 7 Cartoon showing the magmatic development of the upward density increase in Interval 8. **a** Emplacement of a plagioclase-rich crystal mush that produces a proto-anorthosite layer. The pore melt within this crystal mush starts to crystallize pigeonite (Ipx) as it projects towards iron-enrichment. **b** Influx of fresh noritic magma (possibly carrying minor amounts of primocrystic orthopyroxene). This dense noritic magma infiltrates down (*black arrows*) into the resident anorthositic crystal mush, ingesting the resident mush pore melt as it soaks downward. **c** A final solidified profile with a sequence of cumulates that display upwardly increasing density caused by the upward increase in modal pyroxene. Note the presence of corroded/resorbed plagioclase grains (r-Pl) generated during interaction the resident anorthositic mush and a fresh, hotter, invading noritic magma

observe in interval 8, such as increases of up to 10 mol% An at the margins of plagioclase, may be caused by local variations in the abundance of volatiles. Previous work indicates that the Main Zone was volatile-bearing (Willmore et al. 2000). Margin crystallization from small pockets of extreme-bearing pore melt may have produced some of the local extreme zoning.

In summary, the dominantly interstitial texture of orthopyroxene is a function of the pore space available in the resident anorthositic mush into which invading noritic magma crystallized. The lack of evidence to suggest that orthopyroxene has texturally matured suggests that its topology reflects the porosity of the anorthositic mush at the time of magma infiltration, which was likely controlled by the impingement of early-formed primocryst plagioclase laths (Holness 2005). Therefore, although the density contrast and permeability of the resident mush are important, downward infiltration would have also been facilitated by a compositional gradient between the resident mush and the hotter, more mafic, invading magma.

Episodic downward magma infiltration in the Main Zone

Our textural and mineral chemical observations suggest that the initial emplacement of a plagioclase-rich crystal mush, followed by the downward infiltration of noritic magma, can best explain the upward density increase observed in interval 8. There are > 20 cycles in the Bellevue drillcore, throughout the Main and Upper Zones that also show upwardly increasing bulk density. If these cycles were formed by a similar mechanism to that observed in interval 8, then this suggests that the downward infiltration of norite magma was an episodic process during crystallization of the Main Zone. Upward increases in density have also been reported in the Main Zone of the Eastern Limb (Sepato 2014), and await further investigation. There are also cycles in the Bellevue drillcore that show more typical patterns associated with magma fractionation, with cycles showing upwardly decreasing density. These cycles are reminiscent of those produced by the gravitational settling of denser mineral phases during magma crystallization (Cawthorn 2002; Cawthorn and Ashwal 2009). Intervals formed by crystal settling may have been interrupted by cycles that were formed by the initial emplacement of a plagioclase-rich crystal mush and downward magma infiltration. Such alternating differentiation mechanisms suggest a dynamic emplacement environment for BC magmas, regulated by deeper processes in the underlying plumbing system. Upward increases in the primitiveness of mineral compositions similar to what we observe have been documented elsewhere in the BC, including just below the Pyroxenite Marker in the Main Zone (Cawthorn et al.

1991; Nex et al. 2002; VanTongeren and Mathez 2013), as well as in the Merensky Reef footwall unit in the Critical Zone (Maier and Eales 1997). At localities, where upward increases in the primitiveness of mineral compositions, correspond to upward increases in the modal proportion of mafic phases, such cycles may have been formed by the downward infiltration of magma into a resident and semi-consolidated crystal mush. Our model may also have implications for the formation of mineralized zones in this region of the Bushveld Complex (e.g., McDonald et al. 2017)

Wider implications of downward magma infiltration

The downward migration of mafic magma in magma chambers has not previously been proposed as a means of producing cyclic/macro-rhythmic layering on the scale (40–170 m) described in this study. Holness and Vernon (2015) suggested that spontaneous melt infiltration might occur in a melt-free cumulate. Mg-rich exsolution lamellae transcending grain boundaries in Main Zone cumulates of the BC have been documented, and it was suggested that such features were indicative of primitive melt infiltrating a nearly fully-consolidated crystal mush (Roelofse et al. 2009). The presence of reversely zoned plagioclase laths in the uppermost few centimetres of layers in the Cuillin intrusion has been attributed to the downward infiltration of primitive melt (Brandriss et al. 2014). It was also suggested by O'Driscoll et al. (2010) that picritic magmas infiltrated downwards into a troctolite mush during crystallization of the Rum intrusion. In contrast to these models, we observe downward infiltration of magma on a larger scale (~40 m) and mush porosities would have been higher (up to 60%) compared to those suggested in other studies. The importance of downward melt flow has also been documented in volcanic systems with downward melt flow recorded in volcanic feeder dikes (Wadsworth et al. 2015) and in lava lakes (Stovall et al. 2009).

Experimental work on dense fluid interactions with a less dense solid matrix suggests that downward magma infiltration may be an important process in magmatic systems. For example, Hallworth et al. (2005) showed that the top part of an initially homogeneous porous layer of solid crystals will begin to melt when subjected to a heat flux from above, an observation that is consistent with our microstructural evidence. Crystals at the top of this homogeneous layer dissolved, producing a concentrated liquid that is denser than the interstitial liquid below. Convection begins to operate, with denser liquid flowing downward and crystallizing, releasing latent heat and raising the temperature of the lower layer. We envisage, based on our mineral chemical and microstructural observations from interval 8 of the Bellevue drillcore, a similar process to that shown in experiments (Sparks et al. 1985; Hallworth et al. 2005).

However, in our scenario, it is the mixing of different pore melts that facilitates downward magma infiltration. These experiments and our observations from interval 8 illustrate the importance of understanding melt migration processes in magma chambers that are periodically replenished and the potential role of downward magma infiltration in producing layering in large igneous intrusions elsewhere.

Conclusions

The Bellevue drillcore intersects Main and Upper Zone cumulates that are part of the Northern Limb of the Bushveld Complex. Bulk rock density measurements throughout the entire drillcore reveal a scale of layering not previously described in the Bushveld Complex. Layering is characterized by both upward decreases and upward increases in bulk rock density, corresponding to the modal proportion of pyroxene. Upward decreases in density may simply be explained by crystal settling with segregation of dense phases from less dense phases during magma crystallization. However, upward increases in density are the opposite of that predicted by crystal settling. We focused on a ~40 m thick interval displaying an upward increase in density. Textural observations indicate that plagioclase is typically euhedral and appears to have been the main liquidus phase throughout crystallization of the 40 m interval. In contrast, orthopyroxene is dominantly interstitial in texture with local occurrences of euhedral orthopyroxene that are partially resorbed. Interstitial orthopyroxene partly encloses corroded and embayed plagioclase grains. Clinopyroxene is dominantly interstitial and appears to have been the final phase to crystallize. Mineral compositional data indicate that plagioclase and pyroxene compositions are decoupled, with plagioclase molar An content showing no up-section change, while both pyroxene phases show an upward increase in molar Mg# content. Locally, plagioclase laths are reversely zoned, suggesting that these crystals interacted with a more primitive melt during its crystallization. We argue that a significant proportion of plagioclase in the 40 m interval was emplaced as an initial plagioclase-rich mush, explaining its dominantly euhedral lath habit and homogeneous composition. An influx of noritic magma then followed and infiltrated the crystallizing anorthositic crystal mush. Noritic magma that soaked downward would have assimilated increasing proportions of iron-rich pore melt derived from the anorthositic crystal mush, explaining the Mg# trends in pyroxene. Cycles showing upwardly decreasing density that formed by crystal accumulation by gravitational settling were episodically interrupted by cycles of downward magma infiltration during crystallization of the Main and Upper Zones of the Bushveld Complex.

References

Ashwal LD (1993) Anorthosites. Springer-Verlag:422pp

Ashwal LD, Webb SJ, Knoper MW (2005) Magmatic stratigraphy in the Bushveld Northern Lobe: continuous geophysical and mineralogical data from the 2950 m Bellevue drillcore. S Afr J Geol 108(2):199–232. doi:10.2113/108.2.199

Barnes S (1986) The effect of trapped liquid crystallization on cumulus mineral compositions in layered intrusions. Contrib Mineral Petrol 93(4):524–531. doi:10.1007/BF00371722

Barnes S-J, Maier WD, Curl EA (2010) Composition of the marginal rocks and sills of the Rustenburg Layered Suite, Bushveld Complex, South Africa: implications for the formation of the platinum-group element deposits. Econ Geol 105(8):1491–1511

Bédard JH (2007) Trace element partitioning coefficients between silicate melts and orthopyroxene: parameterizations of D variations. Chem Geol 244(1–2):263–303

Bédard JH, Hébert R (1998) Formation of chromitites by assimilation of crustal pyroxenites and gabbros into peridotitic intrusions: North Arm Mountain massif, Bay of Islands ophiolite, Newfoundland, Canada. Journal of Geophysical Research: Solid Earth 103(B3):5165–5184. doi:10.1029/97JB03291

Bédard JH, Sparks RSJ, Renner R, Cheadle MJ, Hallworth MA (1988) Peridotite sills and metasomatic gabbros in the Eastern Layered Series of the Rhum complex (Scotland). Journal - Geological Society (London) 145(2):207–224

Boudreau AE (1988) Investigations of the Stillwater Complex; 4, The role of volatiles in the petrogenesis of the JM Reef, Minneapolis adit section. The Canadian Mineralogist 26(1):193–208

Boudreau AE, Philpotts AR (2002) Quantitative modeling of compaction in the Holyoke flood basalt flow Hartford Basin, Connecticut. Contrib Mineral Petrol 144:176–184

Bowen NL (1928) The evolution of igneous rocks. Princeton University, Princeton

Brandriss ME, Mason S, Winsor K (2014) Rhythmic Layering Formed by deposition of plagioclase Phenocrysts from influxes of porphyritic magma in the Cuillin Centre, Isle of Skye. J Petrol 55(8):1479–1510. doi:10.1093/petrology/egu031

Cameron EN (1980) Evolution of the Lower Critical Zone, central sector, eastern Bushveld Complex, and its chromite deposits. Econ Geol 75(6):845–871. doi:10.2113/gsecongeo.75.6.845

Campbell IH (1977) A Study of macro-rhythmic layering and cumulate processes in the Jimberlana intrusion, Western Australia. Part I: The Upper Layered Series. J Petrol 18(2):183–215. doi:10.1093/petrology/18.2.183

Cawthorn RG (2002) Delayed accumulation of plagioclase in the Bushveld Complex. Mineral Mag 66(6):881–893. doi:10.1180/0026461026660065

Cawthorn RG (2015) The Bushveld Complex, South Africa. In: Charlier B, Namur O, Latypov R, Tegner C (eds) Layered Intrusions, vol. Springer Netherlands, Dordrecht, pp 517–587

Cawthorn RG, Ashwal LD (2009) Origin of anorthosite and magnetitite layers in the bushveld complex, constrained by major element compositions of plagioclase. J Petrol 50(9):1607–1637. doi:10.1093/petrology/egp042

Cawthorn RG, Barton JM, Vilijoen MJ (1985) Interaction of floor rocks with the Platreef on Overysel, Potgietersrus, northern Transvaal. Econ Geol 80:988–1006

Cawthorn RG, Spies L (2003) Plagioclase content of cyclic units in the Bushveld Complex, South Africa. Contrib Mineral Petrol 145(1):47–60. doi:10.1007/s00410-002-0431-0

Cawthorn RG, Webb SJ (2013) Cooling of the Bushveld Complex, South Africa: Implications for paleomagnetic reversals. Geology 41(6):687–690. doi:10.1130/g34033.1

Cawthorn RG, Meyer PS, Kruger FJ (1991) Major Addition of Magma at the Pyroxenite Marker in the Western Bushveld Complex, South Africa. J Petrol 32(4):739–763. doi:10.1093/petrology/32.4.739

Cawthorn RG, Sander BK, Jones IM (1992) Evidence for the trapped liquid shift effect in the Mount Ayliff Intrusion, South Africa. Contrib Mineral Petrol 111(2):194–202. doi:10.1007/BF00348951

Czamanske GK, Bohlen SR (1990) The Stillwater Complex and its anorthosites: an accident of magmatic underplating? Am Mineral 75(1–2):37–45

Eales HV, Costin G (2012) Crustally Contaminated Komatiite: Primary Source of the Chromitites and Marginal, Lower, and Critical Zone Magmas in a Staging Chamber Beneath the Bushveld Complex. Econ Geol 107(4):645–665. doi:10.2113/econgeo.107.4.645

Eales HV, Maier WD, Teigler B (1991) Corroded plagioclase feldspar inclusions in orthopyroxene and olivine of the Lower and Critical Zones, Western Bushveld Complex. Mineral Mag 55:479–486

Finn CA, Bedrosian PA, Cole JC, Khoza TD, Webb SJ (2015) Mapping the 3D extent of the Northern Lobe of the Bushveld layered mafic intrusion from geophysical data. Precambrian Res 268:279–294. doi:10.1016/j.precamres.2015.07.003

Foose MP (1985) Primary structural and stratigraphic relations in Banded-Series cumulates exposed in the East Boulder Plateau-Contact Mountain Area. In: Czamanske GK, Zientek ML (eds) The Stillwater Complex, Montana: geology and guide. Montana Bur Mines and Geol Spec Publ 92:305–324

Hallworth MA, Huppert HE, Woods AW (2005) Dissolution-driven convection in a reactive porous medium. J Fluid Mech 535:255–285. doi:10.1017/S0022112005004830

Hatton CJ (1988) Densities and liquidus temperatures of bushveld parental magmas as constraints on the formation of the Merensky reef. University of Pretoria Institute for Geological Research on the Bushveld Complex

Hayes B, Bédard JH, Lissenberg CJ (2015a) Olivine Slurry Replenishment and the Development of Igneous Layering in a Franklin Sill, Victoria Island, Arctic Canada. J Petrol 56(1):83–112. doi:10.1093/petrology/egu072

Holness MB (2005) Spatial constraints on magma chamber replenishment events from textural observations of cumulates: the Rum Layered Intrusion, Scotland. J Petrol 46(8):1585–1601. doi:10.1093/petrology/egi027

Holness BM, Vernon HR (2015) The Influence of Interfacial Energies on Igneous Microstructures. In: Charlier B, Namur O, Latypov R, Tegner C (eds) Layered Intrusions, vol. Springer Netherlands, Dordrecht, pp 183–228

Humphreys MCS (2009) Chemical evolution of INTERCUMULUS liquid, as recorded in plagioclase overgrowth rims from the Skaergaard Intrusion. J Petrol 50(1):127–145. doi:10.1093/petrology/egn076

Irvine TN (1975) Crystallization sequences in the Muskox intrusion and other layered intrusions—II. Origin of chromitite layers and similar deposits of other magmatic ores. Geochim Cosmochim Acta 39(6–7):991–1020. doi:10.1016/0016-7037(75)90043-5

Kinnaird JA (2005) Geochemical evidence for multiphase emplacement in the southern Platreef. Appl Earth Sci 114(4):225–242. doi:10.1179/037174505X82152

Knoper MW, von Gruenewaldt G (1996) The Bellevue (BV-1) borehole core log: 2.9 km of Bushveld Complex stratigraphy (northern lobe), Potgietersrus, South Africa. Available online at: http://www.geocitiescom/mwkgeo/bichtm

Leuthold J, Blundy JD, Holness MB, Sides R (2014) Successive episodes of reactive liquid flow through a layered intrusion (Unit 9, Rum Eastern Layered Intrusion, Scotland). Contrib Mineral Petrol 168(1):1–27. doi:10.1007/s00410-014-1021-7

Lissenberg CJ, Dick HJB (2008) Melt–rock reaction in the lower oceanic crust and its implications for the genesis of mid-ocean ridge basalt. Earth Planet Sci Lett 271(1–4):311–325. doi:10.1016/j.epsl.2008.04.023

Maier W, Barnes S-J (1998) Concentrations of rare earth elements in silicate rocks of the Lower, Critical and Main Zones of the Bushveld Complex. Chem Geol 150(1):85–103

Maier WD, Barnes SJ, Groves DI (2013) The Bushveld Complex, South Africa: formation of platinum–palladium, chrome- and vanadium-rich layers via hydrodynamic sorting of a mobilized cumulate slurry in a large, relatively slowly cooling, subsiding magma chamber. Miner Deposita 48(1):1–56. doi:10.1007/s00126-012-0436-1

Maier W, Eales HV (1997) Correlation within the UG2-Merensky Reef interval of the western Bushveld Complex, based on geochemical, mineralogical and petrological data. Geological Survey of South Africa, Council for Geoscience

Maier WD, Karykowski BT, Yang S-H (2016) Formation of transgressive anorthosite seams in the Bushveld Complex via tectonically induced mobilization of plagioclase-rich crystal mushes. Geoscience Frontiers 7(6):875–889

Marsh BD (1981) On the crystallinity, probability of occurrence, and rheology of lava and magma. Contrib Mineral Petrol 78(1):85–98. doi:10.1007/BF00371146

McCallum IS (1996) The Stillwater Complex. In: Richard Grant C (ed) Developments in Petrology, vol Volume 15. Elsevier, pp 441–483

McDonald I, Harmer RE, Holwell DA, Hughes HSR, Boyce AJ (2017) Cu-Ni-PGE mineralisation at the Aurora Project and potential for a new PGE province in the Northern Bushveld Main Zone. Ore Geol Rev 80:1135–1159. doi:10.1016/j.oregeorev.2016.09.016

McKenzie D (1984) The Generation and Compaction of Partially Molten Rock. J Petrol 25(3):713–765. doi:10.1093/petrology/25.3.713

Meurer WP, Boudreau AE (1998) Compaction of Igneous Cumulates Part I: Geochemical Consequences for Cumulates and Liquid Fractionation Trends. The Journal of Geology 106:281–292

Mitchell AA, Eales HV, Krueger FJ (1998) Magma replenishment, and the significance of poikilitic textures, in the Lower Main Zone of the western Bushveld Complex, South Africa. Mineral Mag 62(4):435–450

Molyneux TG (1974) A geological investigation of the Bushveld Complex in Sekhukhuneland and part of the Steelpoort Valley. Transactions of the Geological Society of South Africa 77(329–338)

Mondal SK, Mathez EA (2007) Origin of the UG2 chromitite layer, Bushveld Complex. J Petrol 48(3):495–510. doi:10.1093/petrology/egl069

Morse SA (1984) Cation Diffusion in Plagioclase Feldspar. Science 225(4661):504–505. doi:10.1126/science.225.4661.504

Morse S, Nolan KM (1984) Origin of strongly reversed rims on plagioclase in cumulates. Earth Planet Sci Lett 68(3):485–498

Nex PAM, Cawthorn RG, Kinnaird JA (2002) Geochemical effects of magma addition: compositional reversals and decoupling of trends in the Main Zone of the western Bushveld Complex. Mineral Mag 66(6):833–856. doi:10.1180/0026461026660063

O'Driscoll B, Emeleus CH, Donaldson CH, Daly JS (2010) Cr-spinel Seam Petrogenesis in the Rum Layered Suite, NW Scotland: Cumulate Assimilation and in situ Crystallization in a Deforming Crystal Mush. J Petrol 51(6):1171–1201. doi:10.1093/petrology/egq013

O'Hara MJ (1977) Geochemical evolution during fractional crystallization of a periodically refilled magma chamber. Nature 266:503–507

Quadling KE, Cawthorn RG (1994) The layered gabbronorite sequence, Main Zone, eastern Bushveld Complex. S Afr J Geol 97:442–454

Reynolds IM (1985a) The nature and origin of titaniferous magnetite-rich layers in the Upper Zone of the Bushveld Complex: a review and synthesis. Econ Geol 80:1089–1108

Roelofse F, Ashwal LD (2012) The Lower Main Zone in the Northern Limb of the Bushveld Complex—a > 1·3 km Thick Sequence of Intruded and Variably Contaminated Crystal Mushes. J Petrol 53(7):1449–1476. doi:10.1093/petrology/egs022

Roelofse F, Ashwal LD, Pineda-Vargas C, Przyblowicz W (2009) Enigmatic textures developed along plagioclase-augite grain boundaries at the base of the Main Zone, Northern Limb, Bushveld Complex - evidence for late stage melt infiltration into a nearly solidified crystal mush. S Afr J Geol 112:39–46

Scoates JS, Friedman RM (2008) Precise Age of the Platiniferous Merensky Reef, Bushveld Complex, South Africa, by the U-Pb Zircon Chemical Abrasion ID-TIMS Technique. Econ Geol 103(3):465–471. doi:10.2113/gsecongeo.103.3.465

Scoon RN, Mitchell AA (2004) Petrogenesis of Discordant Magnesian Dunite Pipes from the Central Sector of the Eastern Bushveld Complex with Emphasis on the Winnaarshoek Pipe and Disruption of the Merensky Reef. Econ Geol 99(3):517–541. doi:10.2113/gsecongeo.99.3.517

Sepato O (2014) Statistical and wavelet analysis of density and magnetic susceptibility data from the Bushveld Complex, South Africa. MSc Thesis, University of the Witwatersrand

Sharpe MR (1981) The chronology of magma influxes to the eastern compartment of the Bushveld Complex as exemplified by its marginal border groups. J Geol Soc London 138:307–326

Shirley DN (1985) Compaction of igneous cumulates. J Geol 94:795–809

Shirley DN (1987) Differentiation and Compaction in the Palisades Sill, New Jersey. J Petrol 28(5):835–865. doi:10.1093/petrology/28.5.835

Simura R, Ozawa K (2011) Magmatic Fractionation by Compositional Convection in a Sheet-like Magma Body: Constraints from the Nosappumisaki Intrusion, Northern Japan. J Petrol. doi:10.1093/petrology/egr034

Sparks RSJ, Huppert HE, Kerr RC, McKenzie DP, Tait SR (1985) Postcumulus processes in layered intrusions. Geol Mag 122(05):555–568. doi:10.1017/S0016756800035470

Stovall WK, Houghton BF, Harris AJL, Swanson DA (2009) A frozen record of density-driven crustal overturn in lava lakes: The example of Kilauea Iki 1959. Bull Volcanol 71(3):313–318 doi:10.1007/s00445-008-0225-y

Tegner C, Cawthorn RG, Kruger FJ (2006) Cyclicity in the main and upper zones of the Bushveld Complex, South Africa: Crystallization from a zoned magma sheet. J Petrol 47(11):2257–2279

van der Merwe MJ (1978) The geology of the basic and ultramafic rocks of the Potgietersrus Limb of the Bushveld Complex. Unpublished PhD dissertation, University of the Witwatersrand, Johannesburg, South Africa:176pp

VanTongeren JA, Mathez EA (2013) Incoming Magma Composition and Style of Recharge below the Pyroxenite Marker,

Eastern Bushveld Complex, South Africa. J Petrol. doi:10.1093/petrology/egt024

von Gruenewaldt G (1973) The Main and Upper Zones of the Bushveld Complex in the Roossenekal area, eastern Transvaal. Trans Geol Soc South Africa 76:207–227

von Gruenewaldt G (1993) Ilmenite-apatite enrichments in the Upper Zone of the Bushveld Complex: a major titanium-rock phosphate resource. Int Geol Rev 35:987–1000

Wadsworth FB, Kennedy BM, Branney MJ, von Aulock FW, Lavallée Y, Menendez A (2015) Exhumed conduit records magma ascent and drain-back during a Strombolian eruption at Tongariro volcano, New Zealand. Bull Volcanol 77(9):1–10 doi:10.1007/s00445-015-0962-7

Wager LR, Brown GM (1968) Layered igneous rocks. Olivier Boyd, Edinburgh

Webb SJ, Cooper GRJ, Ashwal LD (2015) Wavelet and statistical investigation of density and susceptibility data from the Bellevue drill core and Moordkopje borehole, Bushveld Complex, South Africa. SGA Meeting

Willmore CC, Boudreau AE, Kruger FJ (2000) The Halogen Geochemistry of the Bushveld Complex, Republic of South Africa: Implications for Chalcophile Element Distribution in the Lower and Critical Zones. J Petrol 41(10):1517–1539. doi:10.1093/petrology/41.10.1517

Wilson AH (2012) A Chill Sequence to the Bushveld Complex: Insight into the First Stage of Emplacement and Implications for the Parental Magmas. J Petrol 53(6):1123–1168. doi:10.1093/petrology/egs011

Zeh A, Ovtcharova M, Wilson AH, Schaltegger U (2015) The Bushveld Complex was emplaced and cooled in less than one million years – results of zirconology, and geotectonic implications. Earth Planet Sci Lett 418:103–114. doi:10.1016/j.epsl.2015.02.035